34th Annual International Conference of the IEEE EMBS
San Diego, California USA, 28 August - 1 September, 2012

Multi-Object Active Shape Model Construction for Abdomen Segmentation: Preliminary Results

Sebastian T. Gollmer[1], Martin Simon[2], Arpad Bischof[3], Jörg Barkhausen[4] and Thorsten M. Buzug[1]

Abstract— **The automatic segmentation of abdominal organs is a pre-requisite for many medical applications. Successful methods typically rely on prior knowledge about the to be segmented anatomy as it is for instance provided by means of active shape models (ASMs). Contrary to most previous ASM based methods, this work does not focus on individual organs. Instead, a more holistic approach that aims at exploiting inter-organ relationships to eventually segment a complex of organs is proposed. Accordingly, a flexible framework for automatic construction of multi-object ASMs is introduced, employed for coupled shape modeling, and used for co-segmentation of liver and spleen based on a new coupled shape/separate pose approach. Our first results indicate feasible segmentation accuracies, whereas pose decoupling leads to substantially better segmentation results and performs in average also slightly better than the standard single-object ASM approach.**

I. INTRODUCTION

The upper abdomen presents a wide spectrum of different medical diagnoses. Correspondingly, the segmentation of the important organs that are located in that area, such as liver, spleen, kidney etc. is an issue physicians are often faced with in clinical routine. Such segmentations are for instance useful for computer-based surgery planning, are supportive for diagnosis and monitoring, and can also be used to guide radiation treatments. Commonly, computed tomography (CT) images are acquired for these purposes. These have the problem that the tissue of different organs are represented with quite similar intensity values in the image data. Additionally, pathologies such as tumors and/or previous resections could alter the organs of the individual patient significantly.

The mentioned difficulties makes automatic segmentation of abdominal organs a challenging task that has been extensively studied in recent years. However, the algorithms that have been developed in this context are often tailored for the segmentation of a particular organ like for instance the liver (cf. e.g. [1] and references therein). At this, statistical shape models (SSMs) [2] have proven to be a well-suited tool for shape guided segmentation of individual abdominal organs. Indeed, in the MICCAI 2007 liver segmentation challenge [1], the two best performing automatic segmentation methods [3], [4] are based on this very approach.

On the other hand, there are some works that aim at segmenting two or more abdominal organs based on probabilistic atlases (e.g. [5], [6], [7]). These approaches have shown to be able to provide good segmentation results. Concerning the shape model based approach there are some works that use multi-object SSMs for co-segmentation of different bones [8], [9], brain regions [10], [11] or the epi- and endocardium [12]. However, the much more variable abdominal region has only be addressed in terms of statistical location models [13], i.e. without learning shape variability, or for very local sub-regions of the liver [14], or without benchmarking segmentation results quantitatively [11]. Indeed, the latter aspect got only limited attendance inasmuch as a quantitative evaluation that coupled SSMs can help to improve segmentation results compared to the segmentation of individual organs is until now only conducted for directly connected structures [12], [14] or moderately variable brain regions [10].

Hence, it is quite not clear whether co-modeling of organs like e.g. liver and spleen, which are known to be highly variable and not necessarily connected at all, can actually help to improve segmentation results or if it is more reasonable to segment these organs individually. In order to shed some light onto that question we (i) automatically construct a multi-object SSM comprising liver and spleen using the current quasi-standard for establishing correspondence, (ii) use this model for co-segmentation of both organs, thereby proposing a coupled shape/separate pose approach, and (iii) compare our results with the standard approach in which each organ is segmented individually.

II. MATERIALS AND METHODS

A. Statistical Shape Modeling

Let $\{S_{i,o} \subset \mathbb{R}^3;\, i = 1,\ldots,n_s,\; o = 1,\ldots,n_o\}$ be a set of $n_s \in \mathbb{N}^+$ training samples each consisting of $n_o \in \mathbb{N}^+$ individual objects. By sampling the objects at corresponding positions using $n_{p_o} \in \mathbb{N}^+$ landmarks, we obtain the shape vectors $\mathbf{x}_{i,o} \in \mathbb{R}^{3n_{p_o}}$. These are aligned in a common, normalized coordinate frame. At this, we first align all objects at once to remove global pose differences. Subsequently, we correct for local pose differences by aligning the objects individually [15]. Then, for each sample i, the shape vectors of all objects are concatenated to form a coupled shape vector $\mathbf{x}_i \in \mathbb{R}^{3n_p}$. We calculate the mean shape $\bar{\mathbf{x}} = {n_s}^{-1} \sum_{i=1}^{n_s} \mathbf{x}_i$ as well as the $n_m \in \mathbb{N}$ eigenvalues $\{\lambda_m;\, m = 1,\ldots,n_m\}$ and

[1]S. T. Gollmer and T. M. Buzug are with the Institute of Medical Engineering, University of Lübeck, 23562 Lübeck, Germany {gollmer,buzug}@imt.uni-luebeck.de

[2]M. Simon was with the University Medical Center Schleswig-Holstein, Campus Lübeck, Clinic for Radiology and Nuclear Medicine, 23562 Lübeck, Germany. He is now with the University Medical Center Schleswig-Holstein, Campus Lübeck, Clinic for Neuroradiology, 23562 Lübeck, Germany martin.simon@uk-sh.de

[3]A. Bischof is with the IMAGE Information Systems Ltd., Research Facilities, London, UK bischof@image-systems.biz

[4]J. Barkhausen is with the University Medical Center Schleswig-Holstein, Campus Lübeck, Clinic for Radiology and Nuclear Medicine, 23562 Lübeck, Germany joerg.barkhausen@uk-sh.de

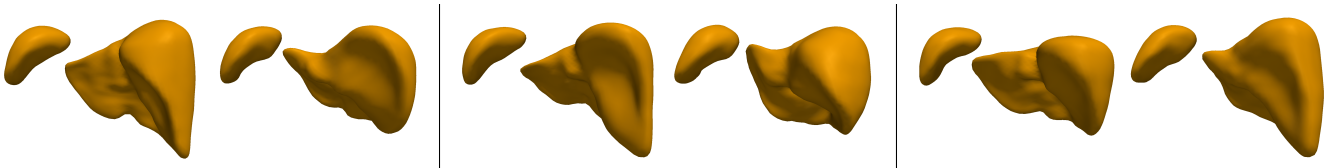

(a) $\mathbf{b}^{(1)} = -3\sqrt{\lambda_1}$ (b) $\mathbf{b}^{(1)} = +3\sqrt{\lambda_1}$ (c) $\mathbf{b}^{(2)} = -3\sqrt{\lambda_2}$ (d) $\mathbf{b}^{(2)} = +3\sqrt{\lambda_2}$ (e) $\mathbf{b}^{(3)} = -3\sqrt{\lambda_3}$ (f) $\mathbf{b}^{(3)} = +3\sqrt{\lambda_3}$

Fig. 1. Coupled shape variability of the multi-object shape model comprising liver and spleen. The displayed shape instances are generated by independently varying the 1st to 3rd mode by -/+ three times the respective standard deviation. In each case the remaining parameters are set to zero.

eigenvectors $\{\mathbf{p}_1,\ldots,\mathbf{p}_{n_m}\}$ of the shape vectors' covariance matrix. $\mathbf{P} = (\mathbf{p}_1 \ldots \mathbf{p}_{n_m})$ spans the coupled shape space and

$$\left\{\mathbf{x} = \bar{\mathbf{x}} + \mathbf{P}\mathbf{b};\ \mathbf{b} \in \mathbb{R}^{n_m}, \mathbf{b}^{(m)} \in \left[-3\sqrt{\lambda_m}, 3\sqrt{\lambda_m}\right]\right\} \quad (1)$$

is the linear statistical shape model with coupled shape parameters $\mathbf{b}$. Note that (1) is a pure shape model that does not contain inter-organ pose variability. By omitting the local alignment of the objects it is also possible to build a pose and shape model [16]. However, given the linear model assumed in this work, the attempt to model e.g. rotational and therewith definitely non-linear effects by this means would amount to corrupt our modeling approach by purpose. Fig. 1 gives a qualitative impression of the coupled shape variability of liver and spleen of the SSM used in this work.

B. Automatic Landmarking

The main challenge in shape modeling is the establishment of corresponding points. While manual landmarking is a feasible approach in 2D, it is impractical in 3D because several thousands of landmarks must be pinpointed exactly on each training sample. In this work, the idea of establishing correspondence by parameterization is adopted and applied to each object to be included in the multi-object ASM. The parameter domain we opt for is the unit-2-sphere $\mathbb{S}^2$. Given such an $\mathbb{S}^2$-parameterization, there exist well-known algorithms for establishing improved correspondence by optimizing a model-based cost function.

The *distmin*-approach [17] is used in order to generate initial parameterizations $\{\omega_{i,o} : \mathbb{S}^2 \to S_{i,o};\ i = 1,\ldots,n_s,\ o = 1,\ldots,n_o\}$. This is motivated by the fact that, as it has been shown recently [17], parameterizations generated in this way are especially suited for subsequent correspondence optimization. This is done based on the algorithm in [18], but using another cost function: The simplified MDL objective is replaced by the approximation of the full MDL cost function [19], which performed superior in our experiments.

C. Texture Modeling

Based on the SSM, an active shape model (ASM) is generated by modeling the local image texture in the vicinity of each landmark and use this learned information to drive the adaption of the model to the image during segmentation. A common approach is to sample 1-D intensity profiles $\{g_i^j\}$ by collecting $2n_a+1$, $n_a \in \mathbb{N}^+$ intensity values with distance Δ along the surface normals $\{\mathbf{n}_i^j\}$ for each landmark j and sample image i. These intensity profiles can directly serve as feature vectors $\{\mathbf{f}_i^j\}$. Assuming that $\{\mathbf{f}_i^j\}$ emanate from a multivariate Gaussian distribution, the average feature vector $\bar{\mathbf{f}}^j = \sum_{i=1}^{n_s} \mathbf{f}_i^j$ and the feature covariance matrix $\mathbf{F}^j = (n_s-1)^{-1}\sum_{i=1}^{n_s}(\mathbf{f}_i^j - \bar{\mathbf{f}}^j)(\mathbf{f}_i^j - \bar{\mathbf{f}}^j)^T$ are used to estimate the probability that the feature vector $\hat{\mathbf{f}}^j$ has been drawn from the modeled distribution using the Mahalanobis distance,

$$d(\hat{\mathbf{f}}^j) = \sqrt{\left(\hat{\mathbf{f}}^j - \bar{\mathbf{f}}^j\right)^T \mathbf{F}^{j^{-1}} \left(\hat{\mathbf{f}}^j - \bar{\mathbf{f}}^j\right)}. \quad (2)$$

The features used in this work combine intensity and gradient profiles. Both are scaled to the interval $[0,1]$ to make them more robust against varying illumination conditions [20] and to ensure their equivalent importance.

D. Image Segmentation

The standard approach for determining the pose parameters $\mathbf{T}$ and the shape parameters $\mathbf{b}$ of the sought segmentation $\mathbf{Y} \in \mathbb{R}^{3n_p}$ is by iteratively minimizing $\mathscr{L} = \sum_{j=1}^{n_p} ||\hat{\mathbf{Y}}^{(j)} - \mathbf{T}\left(\bar{\mathbf{x}}^{(j)} + (\mathbf{P}\mathbf{b})^{(j)}\right)||_2^2$ [2]. To this end, 1-D intensity profiles are sampled from the image volume at positions $\mathbf{a}_j^{(k)} = \mathbf{Y}^{(j)} + k\Delta\mathbf{n}_j;\ k = -n_k,\ldots,n_k, n_k \in \mathbb{N}^+$. Here, $\mathbf{Y}^{(j)} = \mathbf{T}\mathbf{x}^{(j)}$ denotes the position of the j-th landmark in the image space. The fitness of the feature vector $\mathbf{f}^j(\mathbf{a}_j^{(k)})$ is evaluated using (2) and the position of the best performing feature $\hat{\mathbf{f}}^j$ stored in $\hat{\mathbf{Y}}^{(j)}$.

In order to account for the different objects in the multi-object ASM, we propose a *coupled shape/separate pose* approach. That is, given an estimate of the coupled shape parameters $\mathbf{b}$, the pose parameters $\mathbf{T}$ are calculated as in [21] but independently for each object. In this process, outlying feature positions may falsify the pose parameters substantially. Therefore, feature positions with distance $d_j = ||\hat{\mathbf{Y}}^{(j)} - \mathbf{Y}^{(j)}||_2$ greater than the average distance $1/n_p\sum_{j=1}^{n_p} d_j$ are penalized with $1/(2+{d_j}^2)$ [22]. After positioning the objects independently we estimate their coupled shape parameters $\mathbf{b}$ (1) in the least-squares sense as in [2] but using the coupled shape space of all objects (Sec. II-A). This process of separate pose and coupled shape parameter estimation is run for a fixed number of iterations.

III. Experiments and Results

We train a multi-object ASM using 82 abdominal CT scans (in-plane resolution: 0.7-1.0 mm, slice thickness: 3.0-5.0 mm). Manual segmentations of liver and spleen were generated by clinical experts using a tablet monitor and are subsequently used for automatic multi-object SSM construction as detailed in Sections II-A and II-B, whereas 2562/1002 landmarks are used for the liver/spleen. The

TABLE I

MULTI-OBJECT SEGMENTATION ACCURACY USING COUPLED SHAPE AND POSE (CSCP) AND THE NEWLY DEVISED COUPLED SHAPE/SEPARATE POSE (CSSP) APPROACH. VALUES INDICATE MEAN ± STD. ERROR.

	initial	cscp	cssp
ASD / mm	5.9 ± 0.6	4.2 ± 0.2	3.6 ± 0.5
RMSD / mm	7.9 ± 0.9	6.8 ± 0.4	5.7 ± 0.8
VOE / %	29.8 ± 2.4	22.2 ± 1.5	19.0 ± 2.0

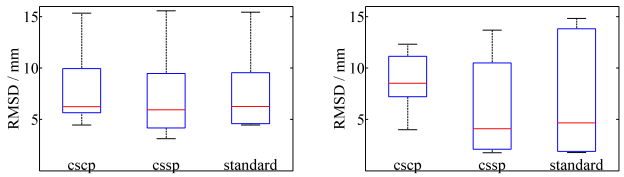

(a) Liver, RMSD (b) Spleen, RMSD

Fig. 2. Segmentation accuracy for individual organs using single-object ASMs (standard) and a multi-object ASM with coupled shape and pose (cscp) and with coupled shape but separate pose (cssp) as devised in this work.

CT scans are smoothed using anisotropic diffusion and an image pyramid comprising four different resolution levels is constructed from the denoised images. At each resolution level and landmark, texture profiles of half length $n_a = 2$ are used (Sec. II-C). The spacing of the profile samples is $\Delta = 4.0/2.0/1.0/0.5$ mm at the different resolution levels.

For testing all five abdominal CT scans (in-plane resolution: 0.6-0.8 mm, slice thickness: 1.3-2.0 mm) from the publicly available 3D-IRCADb-01 database (http://www.ircad.fr/softwares/3Dircadb/3Dircadb1/) that provide manual expert segmentations of both, liver and spleen are used. Equivalently to the training stage, the test images are smoothed using anisotropic diffusion. During segmentation (Sec. II-D), an image pyramid is built and the number of iterations per resolution level is successively increased from 10 to 20. The search radius is set to $n_k = 4$.

We evaluate the proposed multi-object coupled shape/separate pose approach (cssp) w.r.t. the two alternatives (i) coupling of shape and pose (cscp) and (ii) independent segmentation of liver and spleen using two single-object ASMs (standard). In order to have a fair comparison, the initial positioning of the single-object ASMs in a test image must be the same as for the multi-object ASM. Given an appropriate (e.g. manual) initial positioning of the multi-object ASM in the test image, we use the ICP algorithm [23] to calculate the similarity transform that matches the mean shape of the liver and the spleen ASMs with the liver and spleen shape of the initially positioned multi-object ASM.

To compare our results with the manual reference segmentations, the average symmetric surface distance (ASD), the root mean square symmetric surface distance (RMSD), and the volumetric overlap error (VOE) are used. Quantitative and qualitative results are given in Tab. I and in Fig. 2 and 3.

IV. DISCUSSION AND CONCLUSIONS

The quantitative results provided in Tab. I and in Fig. 2 as well as visual inspection of Fig. 3 indicate feasible segmentation results. Clearly, the newly devised coupled shape/separate pose approach provides considerably better results compared to the coupling of shape and pose. This observation applies to both, the multi-object segmentation results (Tab. I) as well as the results for the individual organs (Fig. 2). At this, the spleen benefits more from pose decoupling (Fig. 2(b)) because it is the smaller organ that features less landmarks. Thus, its pose is biased by the more mighty liver in the coupled pose scenario.

Furthermore, Fig. 2 shows that the proposed coupled shape/separate pose approach performs in average slightly better in our tests than the standard procedure of segmenting liver and spleen individually. While this observation applies to both organs, indicating that coupling can indeed help to provide more accurate segmentations of highly variable, not directly connected organs, it might be surprising from a statistical point of view: Given that the number of training samples (here: 82) is typically way smaller than the sample size (here: 7686/3006 for liver/spleen), it seems somewhat counterintuitive that by coupling the samples of different objects, i.e. essentially making the sample size larger, the underlying probabilistic model performs better. Clearly, this aspect needs further investigation by varying (presumably increasing) the size of the training set and the number of modeled objects, and by changing the number of parameters.

The latter aspect can e.g. mean to model the object pose relative to each other. By imposing learned constraints on the inter-organ pose variability rather than estimating the pose solely from the image features, a more robust positioning of the organs might be achieved. As mentioned in Sec. II-A, this amounts to modeling effects that cannot be captured by the linear model (1) but requires alternative methods (e.g. [16]).

In comparison to other works, we have to admit that the atlas based approach of [7] yields more accurate segmentations for liver and spleen. Compared to alternative approaches relying on statistical models for multi-organ segmentation our results are less accurate for the liver than the liver-specific approach in [14]. But we are able to outline liver and spleen more accurate than does the localization model in [13]. At this, it should be noted that the goal of this work is not to provide cutting-edge segmentation results. Instead, the major contribution is the introduction of a general framework for automatic multi-object ASM construction and its application for segmentation in a coupled shape/separate pose scenario.

Our current ASM segmentation basically follows the standard approach, which is prone to fail easily under non-ideal circumstances. For instance, Heimann [24] reported much larger segmentation errors in an application for liver segmentation when using an ASM with linear texture model and linear shape constraints as it is also employed in this work. Contrariwise, the usage of non-linear texture models and less restrictive shape constraints have proven to boost the

(a) Liver (left) and spleen (1st data set, axial) (b) Liver (1st data set, sagittal) (c) Liver (left) and spleen (1st data set, coronal)

(d) Liver (left) and spleen (2nd data set, axial) (e) Spleen (2nd data set, sagittal) (f) Liver (2nd data set, coronal)

Fig. 3. Segmentation results for two data sets using single-object ASMs (black) and the newly devised coupled shape/separate pose approach (white). Manual reference segmentations are marked red. The image intensities are displayed using a standard liver window (window level/width = 30/400 HU).

attainable segmentation results by a factor of two or more [3], [4], [24]. By following these recent approaches, considerable improvements of our current segmentation results can be expected in the near future.

REFERENCES

[1] T. Heimann, B. van Ginneken, M. Styner, and et al., "Comparison and Evaluation of Methods for Liver Segmentation from CT Datasets," *IEEE Trans Med Imaging*, vol. 28, no. 8, pp. 1251–1265, 2009.

[2] T. Cootes, C. Taylor, D. Cooper, and J. Graham, "Active Shape Models – Their Training and Application," *Comp Vis Image Und*, vol. 61, no. 1, pp. 38–59, 1995.

[3] T. Heimann, S. Münzing, H.-P. Meinzer, and I. Wolf, "A Shape-Guided Deformable Model with Evolutionary Algorithm Initialization for 3D Soft Tissue Segmentation," in *IPMI*, 2007, pp. 1–12.

[4] D. Kainmüller, T. Lange, and H. Lamecker, "Shape Constrained Automatic Segmentation of the Liver Based on a Heuristic Intensity Model," in *MICCAI Workshop on 3D Segmentation in the Clinic*, 2007, pp. 109–116.

[5] H. Park, P. Bland, and C. Meyer, "Construction of an Abdominal Probabilistic Atlas and Its Application in Segmentation," *IEEE Trans Med Imaging*, vol. 22, no. 4, pp. 483–492, 2003.

[6] A. Shimizu, R. Ohno, T. Ikegami, H. Kobatake, S. Nawano, and D. Smutek, "Segmentation of Multiple Organs in Non-Contrast 3D Abdominal CT Images," *IJCARS*, vol. 2, no. 3–4, pp. 135–142, 2007.

[7] M. Linguraru, J. Sandberg, Z. Li, F. Shah, and R. Summers, "Automated Segmentation and Quantification of Liver and Spleen from CT Images Using Normalized Probabilistic Atlases and Enhancement Estimation," *Med Phys*, vol. 37, no. 2, pp. 771–783, 2010.

[8] J. Fripp, S. Crozier, S. Warfield, and S. Ourselin, "Automatic Segmentation of the Bone and Extraction of the Bone-cartilage Interface from Magnetic Resonance Images of the Knee," *Phys Med Biol*, vol. 52, no. 6, pp. 1617–1631, 2007.

[9] D. Kainmueller, H. Lamecker, S. Zachow, M. Heller, and H.-C. Hege, "Multi-object Segmentation with Coupled Deformable Models," in *MIUA*, 2008a, pp. 34–38.

[10] A. Akhoundi-Asl and H. Soltanian-Zadeh, "Nonparametric Entropy-based Coupled Multi-shape Medical Image Segmentation," in *ISBI*, 2007, pp. 1200–1203.

[11] A. Tsai, W. Wells, C. Tempany, E. Grimson, and A. Willsky, "Mutual Information in Coupled Multi-shape Model for Medical Image Segmentation," *Med Image Anal*, vol. 8, no. 4, pp. 429–445, 2004.

[12] T. Schwarz, H. T., D. Lossnitzer, C. Mohrhardt, H. Steen, U. Rietdorf, and H.-P. Wolf, Iand Meinzer, "Multiobject Segmentation using Coupled Shape Space Models," in *SPIE*, vol. 7623, 2010.

[13] J. Yao and R. Summers, "Statistical Location Model for Abdominal Organ Localization," in *MICCAI*, vol. 5762, 2009, pp. 9–17.

[14] T. Okada, K. Yokota, M. Hori, M. Nakamoto, H. Nakamura, and Y. Sato, "Construction of Hierarchical Multi-Organ Statistical Atlases and Their Application to Multi-Organ Segmentation from CT Images," in *MICCAI*, vol. 5241, 2008, pp. 502–509.

[15] K. Gorczowski, M. Styner, J.-Y. Jeong, J. Marron, J. Piven, H. Hazlett, S. Pizer, and G. Gerig, "Statistical Shape Analysis of Multi-Object Complexes," in *CVPR*, 2007, pp. 1–8.

[16] M. Bossa and S. Olmos, "Multi-Object Statistical Pose+Shape Models," in *ISBI*, 2007, pp. 1204–1207.

[17] M. Kirschner, S. Gollmer, S. Wesarg, and T. Buzug, "Optimal Initialization for 3D Correspondence Optimization: An Evaluation Study," in *IPMI*, 2011, pp. 308–319.

[18] T. Heimann, I. Wolf, T. Williams, and H.-P. Meinzer, "3D Active Shape Models Using Gradient Descent Optimization of Description Length," in *IPMI*, 2005, pp. 566–577.

[19] R. H. Davies, C. J. Twining, T. F. Cootes, and C. J. Taylor, "Building 3-D Statistical Shape Models by Direct Optimization," *IEEE Trans Med Imaging*, vol. 29, no. 4, pp. 961–981, 2010.

[20] G. Behiels, F. Maes, D. Vandermeulen, and P. Suetens, "Evaluation of Image Features and Search Strategies for Segmentation of Bone Structures in Radiographs Using Active Shape Models," *Med Image Anal*, vol. 6, no. 1, pp. 47–62, 2002.

[21] B. Horn, "Closed-form Solution of Absolute Orientation Using Unit Quaternions," *J Opt Soc Am A*, vol. 4, no. 4, pp. 629–642, 1987.

[22] T. Cootes, A. Hill, C. Taylor, and J. Haslam, "The Use of Active Shape Models for Locating Structures in Medical Images," in *IPMI*, 1993, pp. 33–47.

[23] P. Besl and N. McKay, "A Method for Registration of 3-D Shapes," *IEEE TPAMI*, vol. 14, no. 2, pp. 239–256, 1992.

[24] T. Heimann, "Statistical Shape Models for 3D Medical Image Segmentation," Ph.D. dissertation, University of Heidelberg, 2007.